Eur. Phys. J. B (2022) 95:180
https://doi.org/10.1140/epjb/s10051-022-00446-2

THE EUROPEAN PHYSICAL JOURNAL B

Regular Article - Computational Methods

Investigation of mechanical properties of $KCaH_3$ and $KSrH_3$ orthorhombic perovskite hydrides under high pressure for hydrogen storage applications

Cihan Kurkcu[1], Selgin Al[2,a], and Cagatay Yamcicier[3]

[1] Department of Electronics and Automation, Kirsehir Ahi Evran University, Kırşehir, Turkey
[2] Department of Environmental Protection Technologies, Izmir Democracy University, Izmir, Turkey
[3] Department of Electric and Energy, Osmaniye Korkut Ata University, Osmaniye, Turkey

Received 4 July 2022 / Accepted 21 October 2022 / Published online 3 November 2022

Abstract. First principles calculations have been adopted to explore ground-state and high-pressure properties of $KCaH_3$ and $KSrH_3$ orthorhombic perovskite hydrides for the purpose of solid-state hydrogen storage. Formation enthalpies of materials, structural and mechanical properties, electronic and hydrogen storage properties are computed and examined. The computed formation enthalpies and phonon frequencies of $KCaH_3$ and $KSrH_3$ indicate dynamical stability at 0 GPa. The gravimetric hydrogen densities of $KCaH_3$ and $KSrH_3$ are found to be 3.55 wt% and 2.28 wt%, respectively. Also, the hydrogen desorption temperatures are calculated as 449 K and 394 K for $KCaH_3$ and $KSrH_3$. Elastic constants for each phase and several parameters derived from elastic constants are computed and evaluated, such as bulk and Shear modulus. The B/G ratios of materials depict that both $KCaH_3$ and $KSrH_3$ are brittle materials. The electronic properties show band gaps for both materials at 0 GPa, confirming an insulating nature and as pressure increases the band gap shrinks for $KCaH_3$ and disappears for $KSrH_3$.

1 Introduction

The global energy and climate change crises can be overcome in two ways; one is to find a sustainable, reliable energy source/carrier and the other is to reduce greenhouse gas production/emissions. The perfect solution for these crises would be producing energy from a renewable source and carry it with an effective key energy carrier such as hydrogen. Hydrogen is defined as a reliable, effective, and clean energy carrier by the European Commission [1]. The use of hydrogen as an energy carrier can help to tackle with the challenges of climate change and also meet the goals of international agreements such as Paris Agreement. Hydrogen is abundant (in water and organic compounds), light, and simple. Moreover, it is already used in several applications such as chemical industry, oils, plastics, electronics, fuels, energy conversions via fuel cells or direct internal combustion engines [2].

Currently, most hydrogen production is done via natural gas, coal, biomass, water, and metal hydrides. Although, these conventional procedures are effective ways of producing hydrogen, and can reduce greenhouse gas emissions compared to gasoline, there will be still environmental impacts due to utilising carbon containing source. To produce completely carbon free energy, hydrogen needs to be produced from renewable sources such as wind, solar and even nuclear [3]. For instance, the excess energy which cannot be fed to the grid, from photovoltaic solar panels or wind turbines can be directed to an electrolyser to produce sustainable hydrogen. That way the fluctuations in solar/wind energy and waste of excess energy on sunny days can be avoided and the surplus electricity will be stored and re-electrified when needed. This will also allow one to transfer renewable energy (for example, solar power) from renewable abundant countries such as Brazil, Saudi Arabia and Morocco to areas where the sun light is scarce [1]. The same approach can also be adopted for geothermal/thermal/biomass/nuclear energy to produce sustainable hydrogen at large scales [2]. Producing hydrogen in a green way from renewables can ensure carbon free energy for transportation, aviation, heating, and stationary electricity purposes via fuel cells or hydrogen fuelled internal combustion engines [2]. To use hydrogen in these applications, hydrogen needs to be stored.

There are several methods of storing hydrogen chemically and physically. Physical hydrogen storage includes compressed hydrogen gas tanks, liquid hydrogen tanks and cryogenic tanks. Chemical storage methods include chemical hydrides, metal hydrides and sorbents [2].

[a] e-mail: selgin.al@idu.edu.tr (corresponding author)

Among these multiple hydrogen storage options, solid-state storage of hydrogen has gained a lot attention recently. Several hydrides and catalyst have been under investigation for this purpose. Early research has focused on elemental metal hydrides such as magnesium, lithium and aluminium. Magnesium owns large proportion of publications since it has a moderate 7.6 wt. % hydrogen gravimetric density, cheap and abundant [4, 5]. However, due to the strong bonding between magnesium and hydrogen which causes high dehydrogenation enthalpy 75 kJ/mole, magnesium-based materials are not very practical currently and requires improvement. Aluminium hydride AlH_3, is another great candidate for solid state storage, has great hydrogen storage capacity as 10.1 w.%; however, it is unstable and requires very high pressure to store hydrogen reversibly. YH_2, ZrH_2 and TiH_2 are very stable and thus need very high temperature to work reversibly [6]. Complex metal hydrides such as alanates and borohydrides are also considered for solid state storage. Complex hydrides are promising since they require mild temperature and pressure with reasonable gravimetric hydrogen density. $NaAlH_4$ is a good candidate with a hydrogen content of 5.6 wt.% and inexpensive, but still requires more research and development since they have poor kinetics and require severe conditions for reversibility [7]. Borohydrides have high hydrogen content up to 9.6 wt.% [8], but they have also slow kinetics and borane formation as a by-product [9].

ABH_3 (perovskite-type hydride) has taken attention to store hydrogen recently. Density functional theory which is a proven time and cost-effective way of revealing materials properties, has been utilised intensively to look through these solid-state hydrogen storage candidate materials. A series of 30 new complex perovskite type hydrides are investigated in terms of physical, electronic and hydrogen storage properties [10]. The density functional theory was used to reveal their electronic properties. Another series of 25 perovskite hydrides where A is Li, Na, K, Rb, or Cs, and B is Be, Mg, Ca, Sr, or Ba, is also systematically designed using density functional theory for hydrogen release [11]. Among those, it is reported that Cs-doped $NaCaH_3$ is found to be the most promising material. In the investigation of $LiBaH_3$, $LiSrH_3$ and $LiCsH_3$ by means of first principles calculations, it is reported that the mechanical and phonon densities of $LiBaH_3$ and $LiSrH_3$ are stable which makes them good potential candidates whereas $LiCsH_3$ has showed instability [12]. Li_2MgH_4 with a hydrogen storage capacity 10.52 wt. %, has been investigated in terms of its physical and storage properties under pressure [13]. Li_2MgH_4 has displayed three phases under the pressures of 0 GPa, 5 GPa and 65 GPa, respectively. It illustrated mechanical and dynamic stability at 0 GPa and 5 GPa, however, it is found that Li_2MgH_4 is brittle at 0 GPa, thus it is reported that Li_2MgH_4 seems to have good properties at 5 GPa which makes it a promising material for solid state hydrogen storage. In another study, $KSrH_3$ and $RbSrH_3$ have been considered for hydrogen storage and their structural, mechanical and thermodynamic properties are examined using first principles calculations [14]. $CsCaH_3$ and $RbCaH_3$ have been examined in terms of structural and electronic properties [15]. However, the gravimetric hydrogen densities of these perovskites are lower than the target value 4.5 wt. % set by the US Department of Energy for light-duty fuel cell vehicles [13, 16]. $MgTiH_3$ and $CaTiH_3$ with a hydrogen gravimetric density, 4.01 wt.% and 3.32 wt.%, respectively, has been investigated using first principles calculations [17]. Both materials are metallic, magnetic and stable. MgTiX (X = Ni and Si) is studied; however, dehydrogenation of these materials were found to be low for practical applications [18].

Ternary perovskite hydrides have been under extensive investigation for hydrogen storage since they are mostly light, cheap, abundant and can be used in fuel cells and electrolysers. They also can operate under severe conditions. From this point of view, this study adopts first principles calculations to study $KCaH_3$ and $KSrH_3$ perovskite hydrides in terms of its structural, electronic, mechanical, dynamic and hydrogen storage properties at the ground state. Also, pressure will be applied to the structure to observe potential phase transitions under pressure. Each phase will be examined for its stability via elastic constants. The result will lead us to evaluate these perovskite hydrides as potential solid-state hydrogen hosts. The obtained data will be examined thoroughly and will present new information to the perovskite family.

2 Methods

To study structural, mechanical, electronic and vibrational properties of $KCaH_3$ and $KSrH_3$ perovskite hydrides at the ground state and under pressure, density functional theory (DFT) was adopted to conduct the calculations using the norm-conserving pseudopotential (Troullier-Martins) [19] for K, Ca, Sr and H atoms within SIESTA software package [20]. The calculations were done using double zeta polarized (DZP) basis sets of localized atomic orbitals. The energy mesh cut-off, which defines the spacing of the real space grid utilised to calculate the Hartree, exchange, and correlation contribution to the total energy and Hamiltonian, was set to be 250 Rydberg (Ry). $KCaH_3$ and $KSrH_3$ perovskite hydrides were layout with 2x2x2 cells with periodic boundary conditions for 160 atoms supercells. The Brillouin zones (BZ) were sampled with the6x4x8, and 6 × 8x4 Monkhorst–Pack k-point mesh for the orthorhombic Pnma and the monoclinic Cc and C2/m phases, respectively [21]. Structural optimizations were completed using the conjugate gradient technique until the residual force acting on all atoms was smaller than 0.01 eV/Å and the pressure was gently rose by 10 GPa through this technique to the system. $KCaH_3$ and $KSrH_3$ compounds were first equilibrated after optimisation and then pressure was increased with an increment of 10 GPa up to a pressure value of 150 GPa (0,

10, 20, 30 ... 150 GPa). The length of time elapsed at each pressure value applied in this study ends when the structure reaches equilibrium. Phase transition was observed when a pressure of 40 GPa was applied on the structure. At this pressure value where the phase transition occurs, the structure has reached equilibrium after 487 cycle movements and approximately 88 h. The structure was equilibrated at each applied pressure through 1 femto second (fs:10^{-15} s) time step. The process started from the beginning at each pressure step from the equilibrated coordinates of previous steps to make sure the pressure path to be continuous. To analyse each minimization time, KPlot program was adopted and the RGS algorithm which gives detailed information about the space groups, atomic positions and lattice parameters of an analysed structure [22, 23]. For the energy-volume calculations, the unit cells of the Pmmn, Cc and C2/m phases were adopted.

3 Results and discussion

3.1 Formation enthalpy

Formation enthalpy is a critical parameter which demonstrates stability of the material with regards to decomposition to its components. It will be useful to evaluate the materials ability either it is suitable for practical applications or not. The formation enthalpies of materials are calculated at 0 K as follows:

$$\Delta H_F = E_T(KXH_3) - \left[E(K) + E(X) - \frac{3}{2}E(H_2)\right], \tag{1}$$

$E_T(KXH_3)$ presents total energy of KXH_3 (X = Ca, Sr), $E(K)$ and $E(X)$ presents the ground state energies of K and X, and $E(H_2)$ stands for ground state energy of hydrogen. The calculated formation energy for $KCaH_3$ is − 0.608 eV/atom and for $KSrH_3$ is − 0.534 eV/atom. The negative values of materials display dynamically stability as well as synthesizability.

3.2 Gravimetric hydrogen storage density and desorption temperature

To define possible adoption of these materials for hydrogen storage, gravimetric hydrogen density capacities and hydrogen desorption temperature is calculated. Gravimetric hydrogen density (GHD) is computed using the equation below [24].

$$C_{wt\%} = \left(\frac{(H/M)M_H}{M_{Host} + (H/M)M_H} \times 100\right)\%, \tag{2}$$

H/M presents metal to hydrogen ratio and M_{Host} and M_H presents molar mass of the host material and hydrogen. Based on the calculations, the GHD of $KCaH_3$ is found to be 3.55 wt.% and $KSrH_3$ is found to be 2.28 wt. %.

Another important parameter is hydrogen desorption temperature from the host material. These values are also estimated using the equation below.

$$\Delta H = T_d \times \Delta S, \tag{3}$$

where T_d is hydrogen desorption temperature and ΔS is the hydrogen entropy change which is previously determined as 130.7 J/mol. K [13, 25]. The hydrogen desorption temperature for $KCaH_3$ is found to be 449 K and 394 K for $KSrH_3$. This temperature range is considered to be achievable even for portable practical applications [4].

3.3 Structural evolution

The ground-state structures of $KCaH_3$ and $KSrH_3$ are determined as orthorhombic Pnma after optimisation at zero pressure and temperature. The lattice parameters (Å) are found to be for $KCaH_3$; a = 6.5426, b = 9.1865, c = 6.4748 and for $KSrH_3$; a = 6.9098, b = 9.6234, c = 6.7367. The volume changes in the simulation cells are given in Fig. 1. As Fig. 1 shows, there are sharp volume collapses for both materials. $KCaH_3$ undergoes a phase transition at 50 GPa from Pnma orthorhombic to Cc monoclinic structure whereas $KSrH_3$ undergoes a phase transition at 40 GPa from Pnma orthorhombic to C2/m monoclinic structure. The dramatic change in volumes indicate first order phase transition. The atomic positions of phases are also simulated and given in Fig. 2.

The constant pressure calculations can result in estimation of higher transition pressure with respect to actual experimental conditions and greater activation energy barrier for phase transitions due to short timescales, perfect boundary conditions etc. [26–30]. Therefore, Gibbs free energy concept is also adopted to calculate phase transitions of the materials where the stable structure has the lowest Gibbs free energy:

$$\mathrm{G} = \mathrm{E_{tot}} + \mathrm{PV} - \mathrm{TS}, \tag{4}$$

where $\mathrm{E_{tot}}$, P, V, T, and S represents the total internal energy, pressure, volume, temperature and entropy. At 0 K, the equation becomes the enthalpy, H:

$$\mathrm{H} = \mathrm{E_{tot}} + \mathrm{PV}. \tag{5}$$

To obtain enthalpy of phases of materials, energies for phases for different volumes are computed by scaling the lattice parameters and atomic positions uniformly and the result is given in Fig. 3. Then the obtained data are fitted to the third-order Birch-Murnaghan equation of state [31, 32] given below:

$$\mathrm{P} = 1.5\mathrm{B_0}\left[\left(\frac{\mathrm{V}}{\mathrm{V_0}}\right)^{-\frac{7}{3}} - \left(\frac{\mathrm{V}}{\mathrm{V_0}}\right)^{-\frac{5}{3}}\right]$$

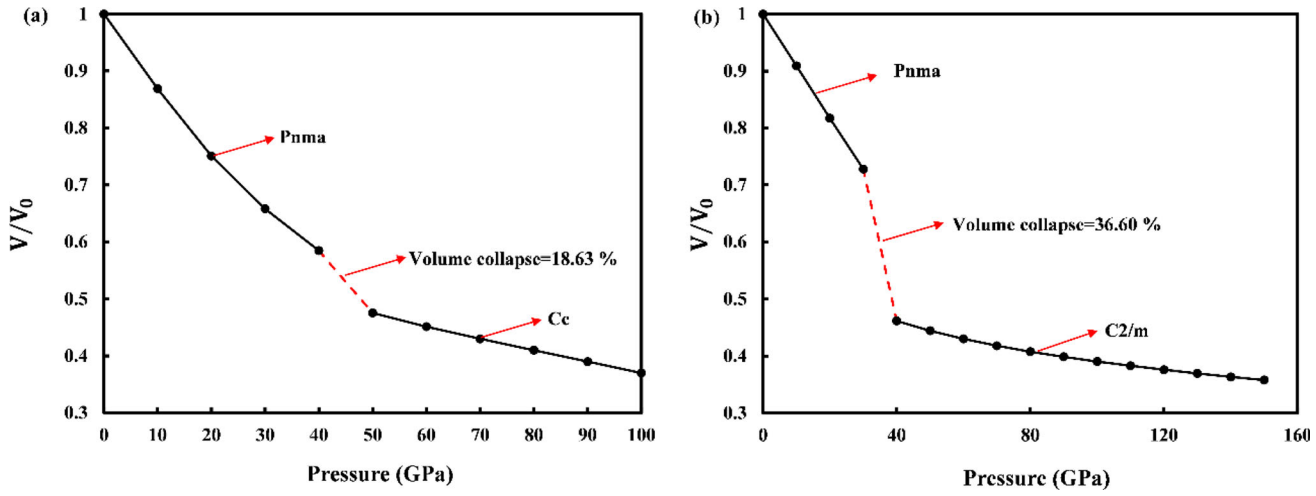

Fig. 1 The changes in volumes under pressure a) $KCaH_3$ and b) $KSrH_3$

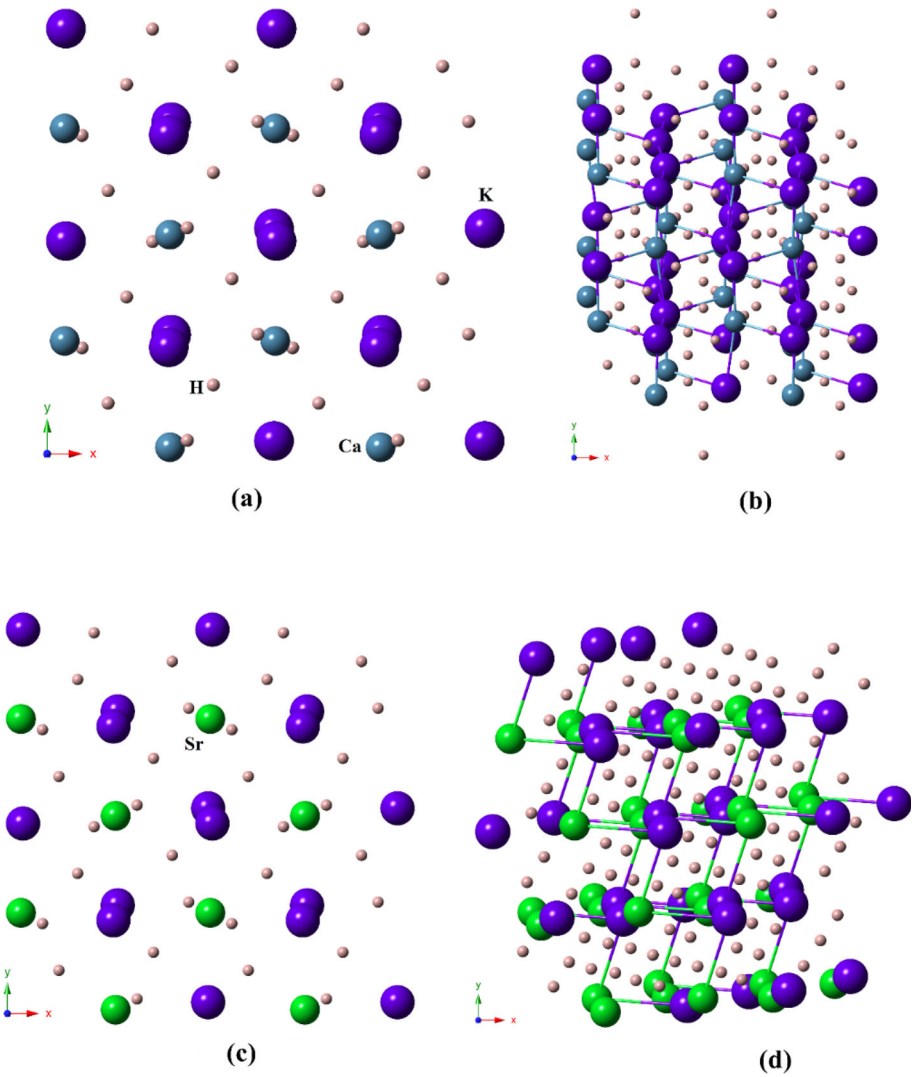

Fig. 2 Crystal structures of $KCaH_3$ a) Pnma at 0 GPa b) Cc at 50 GPa, $KSrH_3$ c) Pnma at 0 GPa, d) C2/m at 40 GPa

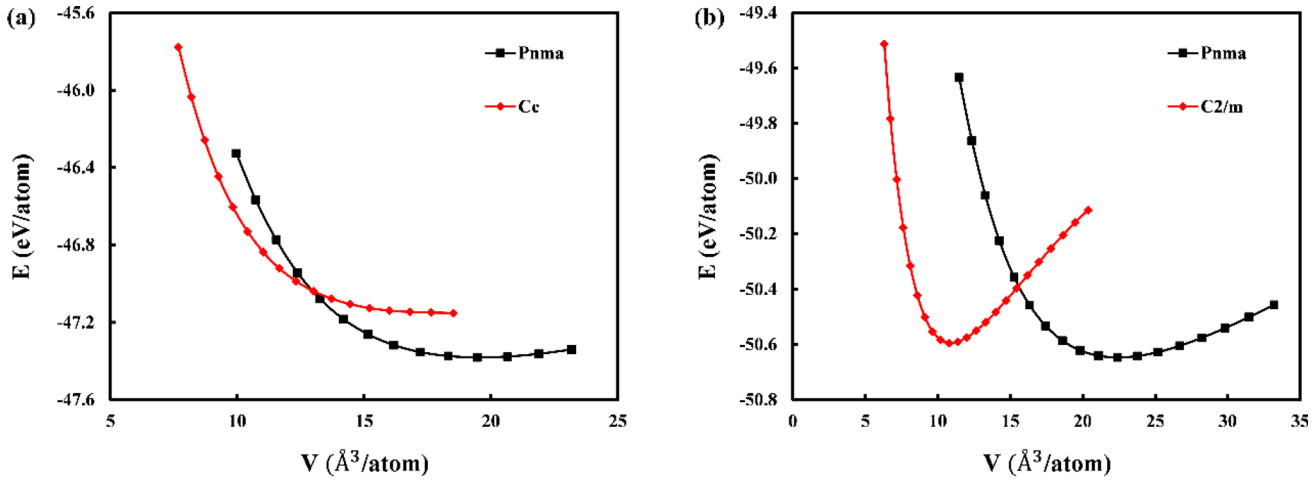

Fig. 3 The changes in energy-volume for phases of **a** $KCaH_3$ and **b** $KSrH_3$

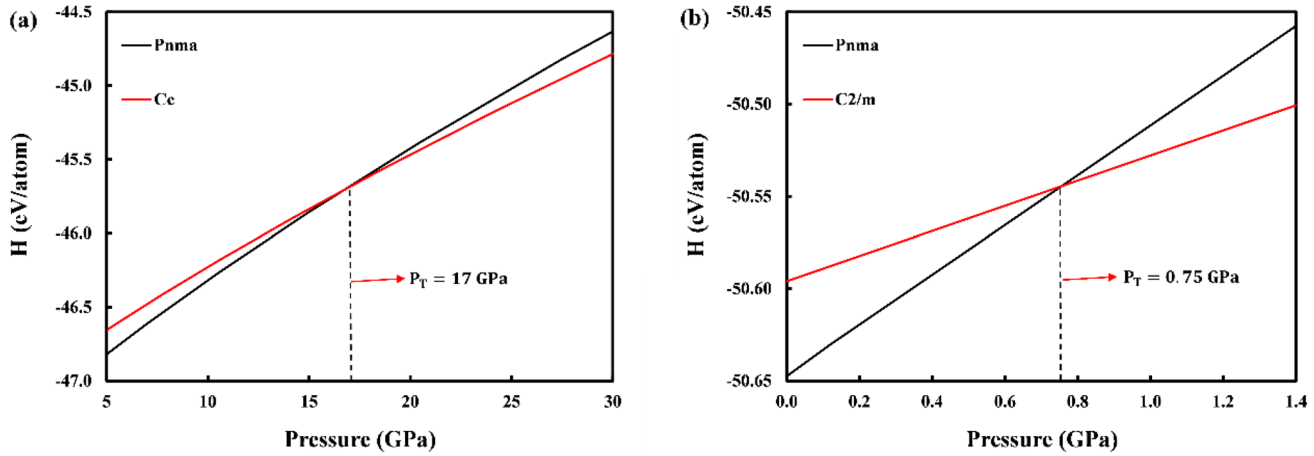

Fig. 4 The variations in enthalpy for phases of **a** $KCaH_3$ and **b** $KSrH_3$

$$x\left\{1+0.75\left(B_0^{'}-4\right)\left[\left(\frac{V}{V_0}\right)^{-\frac{2}{3}}-1\right]\right\}, \quad (6)$$

where P, V,V_0, B_0 and $B_0^{'}$ are pressure, volume at given pressure and the volume, bulk modulus and its pressure derivate at 0 GPa, respectively.

From that P as $P = dE_{tot}/dV$ and finally the enthalpy values of phases can be computed. The stable phase will have the lowest enthalpy at 0 K and a known pressure. Both phases will have the same enthalpy when a phase transition take places. The computed enthalpies of materials are given in Fig. 4. As can be seen from Fig. 4 that the enthalpies of $KCaH_3$ cross each other at 17 GPa, indicating that $KCaH_3$ transforms from Pnma to Cc at 17 GPa and the enthalpies of $KSrH_3$ cross at 0.75 GPa, suggesting that $KSrH_3$ undergoes a phase transition at 0.75 GPa. One can note from Fig. 4 that, below the transition pressures, Pnma phases of materials have lowest enthalpies, suggesting that Pnma phases are thermodynamically and mechanically more stable. It should also be noticed that beyond the transition pressures, the enthalpies of Cc and C2/m phases become slightly more negative, indicating that when the pressure increases Cc and C2/m phases become more stabilized.

3.4 Elastic properties

The mechanical and elastic properties of $KCaH_3$ and $KSrH_3$ are essential to test the suitability of these materials for practical applications in terms of stability and durability. The elastic constants along with other parameters derived from elastic constants of $KCaH_3$ and $KSrH_3$ are given in Tables 1, 2, 3 and 4. There are nine independent elastic constants for orthorhombic symmetry which are numerically estimated and presented in Tables 1 and 3 for $KCaH_3$ and $KSrH_3$. The mechanical stability evaluation has been carried out based on the Born stability criteria for orthorhombic

Table 1 Elastic constants (GPa) of $KCaH_3$ phases

Phases	C_{11}	C_{12}	C_{13}	C_{15}	C_{22}	C_{23}	C_{25}	C_{33}	C_{35}	C_{44}	C_{55}	C_{66}
Pnma	38.86	11.59	9.21	–	35.61	11.69	-	39.67	–	15.82	12.33	17.01
Cc	195.20	70.18	54.56	– 28.36	146.84	63.08	13.25	191.66	– 14.36	50.06	53.32	43.69

Table 2 The calculated Bulk modulus (B, GPa), Shear modulus G (GPa), G/B and B/G ratios, Poisson's ratios (σ) and Young's modulus E (GPa) of $KCaH_3$ phases

Phases	*B*	*G*	*G /B*	*B/G*	*σ*	*E*
Pnma	19.90	14.35	0.721	1.387	0.209	34.70
Cc	100.01	49.46	0.494	2.022	0.288	127.39

Table 3 Elastic constants (GPa) of $KSrH_3$ phases

Phases	C_{11}	C_{12}	C_{13}	C_{22}	C_{23}	C_{33}	C_{44}	C_{55}	C_{66}
Pnma	36.19	9.17	8.99	29.47	9.50	33.98	11.05	10.82	12.13
C2/m	839.05	– 94.56	737.17	1684.32	– 10.82	– 481.90	– 452.65	93.83	– 2410.51

symmetry [33, 34];

$$\begin{aligned} &C_{11}+C_{33}-2C_{13}>0, C_{22}+C_{33}-2C_{23}>0,\\ &C_{11}+C_{22}-2C_{12}>0,\\ &\quad C_{11}>0, \quad C_{22}>0, \quad C_{33}>0, \quad C_{44}>0,\\ &\quad C_{55}>0, \quad C_{66}>0,\\ &C_{11}+C_{22}+C_{33}+2(C_{12}+C_{13}+C_{23})>0,\\ &1/3(C_{12}+C_{13}+C_{23})<B<(C_{11}+C_{22}+C_{33}). \end{aligned} \tag{7}$$

At 0 GPa, the determined elastic constants of $KCaH_3$ and $KSrH_3$ satisfy the mechanical stability criteria given in Eq. 7, indicating that Pnma phase of $KCaH_3$ and $KSrH_3$ are mechanically stable. Unfortunately, there are no existing data for comparison, thus this study and data might serve as a reference for future studies.

C_{11}, C_{22}, C_{33} describe the linear compression along crystallographic axis and the nature of atomic bonding [35]. For $KCaH_3$, it can be seen from Table 1 that $C_{33} > C_{11} > C_{22}$. This suggests that the interatomic bonding along the (010) planes is much delicate than that of (001) and (100) planes. For $KSrH_3$, it seen from Table 3 that $C_{11} > C_{33} > C_{22}$. For both materials, the (010) plane is much sensitive to external deformations than (001) and (100) planes. Thus, hydrogens from (010) plane will be released much easily compared to (100) and (001) plane hydrogens. Also, C_{44}, C_{55} and C_{66} reflect to shear deformation. For both materials, it is seen that C_{11}, C_{22}, C_{33} are higher than C_{44}, C_{55} and C_{66}, indicating that orthorhombic $KCaH_3$ and $KSrH_3$ depict much resistance to unidirectional compression than shear deformation.

Under pressure, $KCaH_3$ and $KSrH_3$ transforms into monoclinic Cc and C2/m structures, respectively. Their elastic constants are also computed and examined. For a monoclinic structure, the well-known Born stability criteria is given as [36, 37]

$$\begin{aligned} &C_{33}C_{55}-C_{32}^2>0, C_{44}C_{66}-C_{46}^2>0,\\ &\quad C_{22}+C_{33}-2C_{23}>0 C_{11}+C_{22}+C_{33}\\ &+2(C_{12}+C_{13}+C_{23})>0\\ &C_{22}(C_{33}C_{55}-C_{35}^2)+2C_{23}C_{25}C_{35}-C_{23}^2C_{55}-C_{25}^2C_{33}>0,\\ &2[C_{15}C_{25}(C_{33}C_{12}-C_{13}C_{23})+C_{15}C_{35}(C_{22}C_{13}-C_{12}C_{23})\\ &\quad +C_{25}C_{35}(C_{11}C_{23}-C_{12}C_{13})]-[C_{15}^2(C_{22}C_{33}-C_{23}^2)\\ &\quad +C_{25}^2(C_{11}C_{33}-C_{13}^2)+C_{35}^2(C_{11}C2_2-C_{12}^2)]+gC_{55}>0,\\ &\quad \text{With g}=C_{11}C_{22}C_{33}-C_{11}C_{23}^2-C_{22}C_{13}^2\\ &-C_{33}C_{12}^2+2C_{12}C_{13}C_{23}. \end{aligned} \tag{8}$$

Based on Tables 1 and 3, it is seen that monoclinic phases $KCaH_3$ and $KSrH_3$ do not meet the criteria given in Eq. 8, thus these phases are not mechanically stable.

It is noteworthy to calculate elastic properties of orthorhombic phases of $KCaH_3$ and $KSrH_3$ such as bulk modulus, shear modulus, Poisson's ratio, and Young modulus to evaluate their future use for hydrogen storage. Therefore, we further calculated elastic properties of orthorhombic phases of $KCaH_3$ and $KSrH_3$ using elastic constants (details of calculation is given in [38]) presented in Tables 2 and 4.

Generally, bulk modulus of materials reflect its ability to resist volume alterations under external pressure [39]. As bulk modulus increases, the resistance becomes much larger against volume change. The obtained bulk modulus of $KCaH_3$ is higher than that of $KSrH_3$, indicating that it will be much difficult to compress $KCaH_3$ than $KSrH_3$. Shear modulus corresponds to shear resistance to shearing force, the larger shear modulus means the higher shear resistance [38]. By comparing shear modulus of two materials, it can be said that $KCaH_3$

Table 4 The calculated Bulk modulus (B, GPa), Shear modulus G (GPa), G/B and B/G ratios, Poisson's ratios (σ) and Young's modulus E (GPa) of $KSrH_3$ phases

Phases	*B*	*G*	*G/B*	*B/G*	*σ*	*E*
Pnma	17.17	11.56	0.673	1.485	0.225	28.32
C2/m	313.56	393.25	1.254	0.797	0.058	831.96

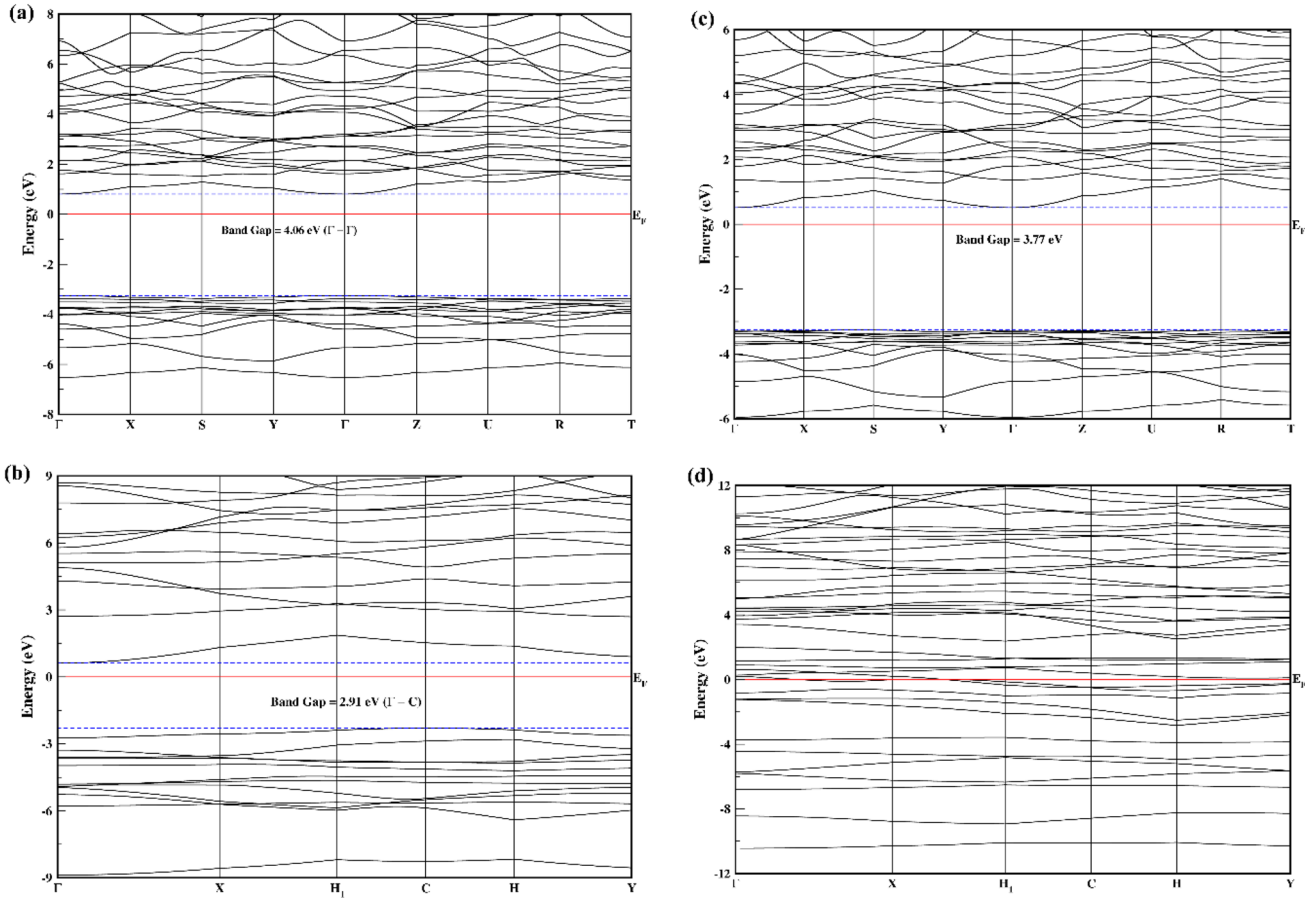

Fig. 5 Calculated electronic structures of $KCaH_3$ **a** Pnma at 0 GPa **b** Cc at 50 GPa, $KSrH_3$ **c** Pnma at 0 GPa, **d** C2/m at 40 GPa

will also show higher resistance towards shear deformation. Also, Young modulus is given as the ratio between stress to strain and defines solid stiffness, as Young modulus increases, the material's stiffness increases. $KCaH_3$ has slightly higher Young modulus than $KSrH_3$, indicating that $KCaH_3$ has better stiffness than $KSrH_3$.

The brittleness and ductility of materials can be examined via the bulk to shear modulus ratio (B/G) and Poisson's ratio (σ). As suggested by Pugh [40] if B/G is higher than 1.75, the material is ductile otherwise the material is described as brittle. Based on the data given in Tables, both materials are brittle in nature which can be an obstacle when handling the materials and it may require extra attention for non-stationary applications. Poisson's ratio can be used to describe bonding characteristics. This ratio is proposed as 0.1 for covalent materials and 0.25 for ionic materials in the literature [41]. The Poisson's ratios of materials given Tables 2 and 4 demonstrate that both materials have dominant ionic bonding characteristics.

3.5 Band and phonon structures

The calculated electronic band structures of $KCaH_3$ and $KSrH_3$ for Pnma, *Cc* and $C2/m$ phases along with the high symmetry directions are given in Fig. 5. For all, Fermi energy is levelled at the top of the valence band (VB) and adjusted to 0 eV. As Fig. 5 shows that $KCaH_3$ has band gaps in both phases as 4.06 eV at 0 GPa (Pnma phase) and 2.91 eV at 50 GPa (Cc phase), indicating that $KCaH_3$ is an insulator at all pressures. On the other hand, $KSrH_3$ has a band gap as 3.77 eV

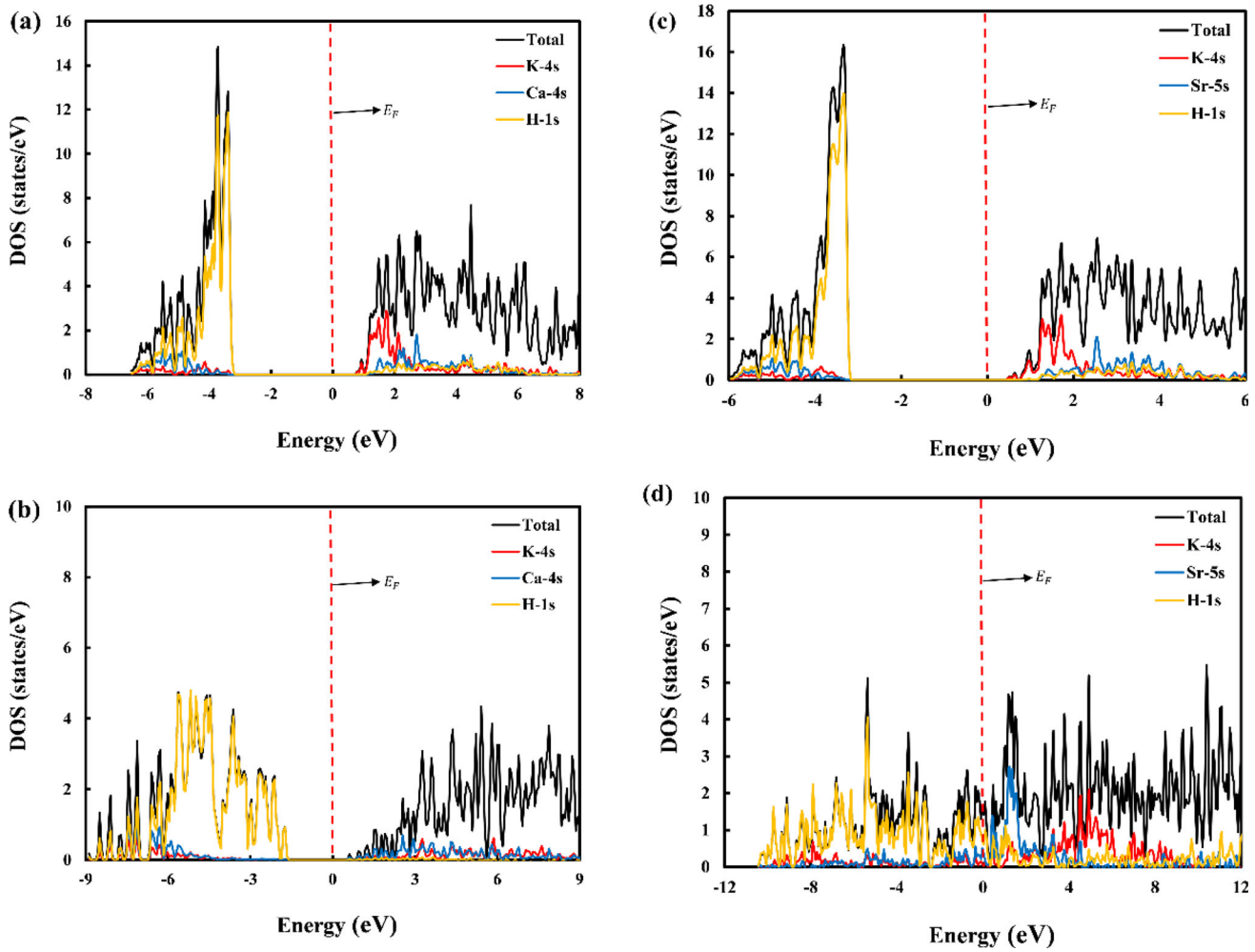

Fig. 6 Calculated electronic density of states for $KCaH_3$ **a** Pnma at 0 GPa **b** Cc at 50 GPa, $KSrH_3$ **c** Pnma at 0 GPa, **d** C2/m at 40 GPa

at 0 GPa (Pnma phase) and no band gap at 40 GPa (C2/m phase). As the pressure increases, valence band near the band gap seems to shift higher energies gradually whilst conduction band seems to shift lower energies. $KSrH_3$ behaves like an insulator at 0 GPa and becomes a conductor as phase transition occurs at 40 GPa.

Figure 6 depicts the energy dependence of DOS of $KCaH_3$ and KSrH3 for Pnma, Cc and $C2/m$ phases. H-1 s orbit electrons seem to be dominant in valence band with a little contribution from Ca-4 s orbit electrons whereas K-4 s and Ca-4 s orbit electrons contribute to the conduction band for $KCaH_3$. For $KSrH_3$, as the pressure increases, the band gap energy decreases. At 0 GPa, H-1 s orbit electrons are dominant in the valence band and K-4 s orbit electrons become dominant at the conduction band as the pressure increases.

The phonon dispersion curves of $KCaH_3$ and $KSrH_3$ at 0 GPa are also computed and presented in Fig. 7. The phonon curves show that there is no imaginary frequency (all phonon frequencies are positive) exist in both figures, indicating that both materials at 0 GPa are dynamically stable.

4 Conclusions

The aim of this study is to investigate ground state properties and phase transitions under high pressure of $KCaH_3$ and $KSrH_3$ perovskite hydrides. First, the formation enthalpies of materials are calculated as -0.608 eV/atom for $KCaH_3$ and − 0.534 eV/atom for $KSrH_3$. Then, the GHD of $KCaH_3$ and $KSrH_3$ is found to be 3.55 wt.% and 2.28 wt. %, respectively. Also, hydrogen desorption temperatures are obtained as 449 K for $KCaH_3$ and 394 K for $KSrH_3$. As pressure increases it seen that $KCaH_3$ undergoes a phase transition at 50 GPa from Pnma orthorhombic to Cc monoclinic structure and $KSrH_3$ undergoes a phase transition at 40 GPa from Pnma orthorhombic to C2/m monoclinic structure. The mechanical properties and stabilities of materials are also examined. It is seen that Pnma

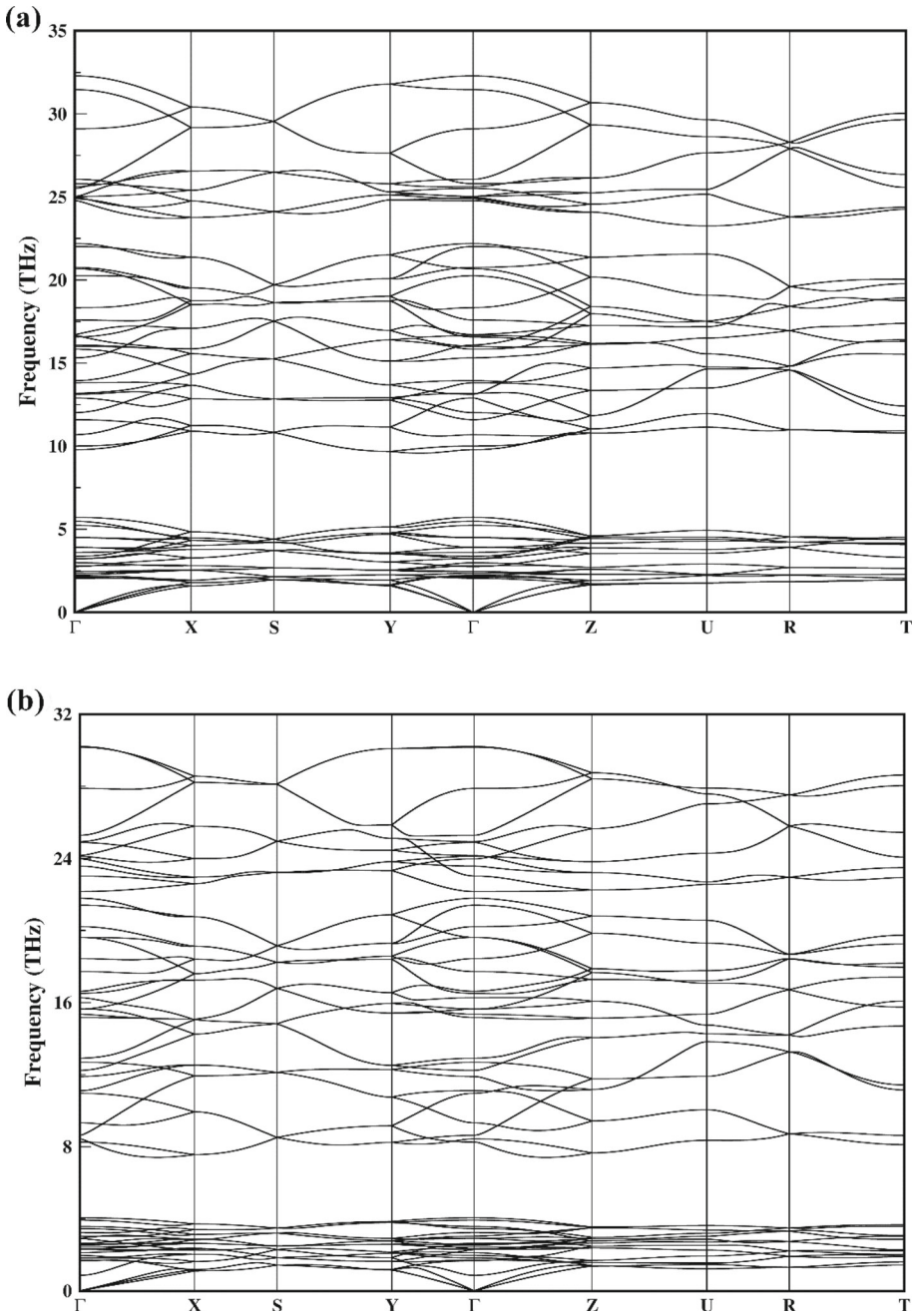

Fig. 7 The phonon dispersion curves of **a** $KCaH_3$ and **b** $KSrH_3$ at 0 GPa

phases of materials are stable based on the Born stability criteria, however, Cc and C2/m phases of materials are not stable. Formation enthalpies and phonon frequencies at 0 GPa indicate dynamic stability. Several properties such as ductility and brittleness of materials are evaluated based on the elastic constants. The B/G ratios of materials confirm that both materials are brittle. The electronic properties show insulating character for both materials at 0 GPa. $KSrH_3$ becomes a conducting material with the phase change under pressure.

Author contributions

All authors contributed equally to the preparation of the manuscript.

Data availability statement This manuscript has no associated data or the data will not be deposited. [Authors' comment: The data that support the findings of this study are available from the corresponding author upon reasonable request.]

References

1. M. Hirscher et al., *Materials* for *hydrogen-based energy storage – past, recent progress and future outlook*. J. Alloy. Compd. **827**, 153548 (2020)
2. A.G. Olabi et al., Large-scale hydrogen production and storage technologies: Current status and future directions. Int. J. Hydrogen Energy **46**(45), 23498–23528 (2021)
3. Irena, H., *A renewable energy perspective*. J IRENA, Abu Dhabi, 2019.
4. V.A. Yartys et al., Magnesium based materials for hydrogen based energy storage: Past, present and future. Int. J. Hydrogen Energy **44**(15), 7809–7859 (2019)
5. J.-C. Crivello et al., Review of magnesium hydride-based materials: development and optimisation. J Applied Physics A **122**(2), 1–20 (2016)
6. I.A. Hassan et al., Hydrogen storage technologies for stationary and mobile applications: Review, analysis and perspectives. Renew. Sustain. Energy Rev. **149**, 111311 (2021)
7. D.A. Mosher et al., Design, fabrication and testing of $NaAlH_4$ based hydrogen storage systems. J. Alloy. Compd. **446–447**, 707–712 (2007)
8. Y. Kojima, Hydrogen storage materials for hydrogen and energy carriers. Int. J. Hydrogen Energy **44**(33), 18179–18192 (2019)
9. G. Barkhordarian et al., Unexpected kinetic effect of MgB_2 in reactive hydride composites containing complex borohydrides. J. Alloy. Compd. **440**(1), L18–L21 (2007)
10. P. Schouwink et al., Structure and properties of complex hydride perovskite materials. J Nature communications **5**(1), 1–10 (2014)
11. Y. Li, J.S. Chung, S.G. Kang, First-Principles Computational Screening of Perovskite Hydrides for Hydrogen Release. J ACS combinatorial science **21**(11), 736–742 (2019)
12. H.H. Raza et al., Optoelectronic and thermal properties of $LiXH_3$(X = Ba, Sr and Cs) for hydrogen storage materials: A first principle study. Solid State Commun. **299**, 8 (2019)
13. S. Al, C. Kurkcu, C. Yamcicier, High pressure phase transitions and physical properties of Li_2MgH_4; implications for hydrogen storage. Int. J. Hydrogen Energy **45**(7), 4720–4730 (2020)
14. H.H. Raza et al., First-principle investigation of $XSrH_3$ (X = K and Rb) perovskite-type hydrides for hydrogen storage. Int. J. Quantum Chem. **120**(24), e26419 (2020)
15. S. Lamichhane et al., Structural and electronic properties of perovskite hydrides $ACaH_3$ (A= Cs and Rb). J BIBECHANA **13**, 94–99 (2016)
16. 2022 [cited 2022 12.09.2022]; Available from: https://www.energy.gov/eere/fuelcells/doe-technical-targets-onboard-hydrogen-storage-light-duty-vehicles.
17. Al, S., *Investigations of Physical Properties of $XTiH_3$ and Implications for Solid State Hydrogen Storage*, in *Zeitschrift für Naturforschung A*. 2019. p. 1023.
18. Manivasagam, T.G., et al., *Synthesis and electrochemical properties of binary MgTi and ternary MgTiX (X= Ni, Si) hydrogen storage alloys*. 2017. **42**(37): p. 23404–23415.
19. N. Troullier, J.L. Martins, Efficient pseudopotentials for plane-wave calculations. Phys. Rev. B **43**(3), 1993 (1991)
20. P. Ordejón, E. Artacho, J.M. Soler, Self-consistent order-N density-functional calculations for very large systems. Phys. Rev. B **53**(16), R10441 (1996)
21. H.J. Monkhorst, J.D. Pack, Special points for Brillouin-zone integrations. Phys. Rev. B **13**(12), 5188 (1976)
22. R. Hundt et al., Determination of symmetries and idealized cell parameters for simulated structures. J. Appl. Crystallogr. **32**(3), 413–416 (1999)
23. A. Hannemann et al., A New Algorithm for Space-Group Determination. J. Appl. Crystallogr. **31**(6), 922–928 (1998)
24. S. Al, C. Kurkcu, C. Yamcicier, Structural evolution, mechanical, electronic and vibrational properties of high capacity hydrogen storage TiH_4. Int. J. Hydrogen Energy **45**(55), 30783–30791 (2020)
25. Q. Zeng et al., Evaluation of the Thermodynamic Data of CH_3SiCl_3 Based on Quantum Chemistry Calculations. J. Phys. Chem. Ref. Data **35**(3), 1385–1390 (2006)
26. C. Yamcicier, Z. Merdan, C. Kurkcu, Investigation of the structural and electronic properties of CdS under high pressure: an ab initio study. Can. J. Phys. **96**(2), 216–224 (2017)
27. C. Kürkçü et al., Investigation of structural and electronic properties of β-HgS: Molecular dynamics simulations. Chin. J. Phys. **56**(3), 783–792 (2018)
28. M. Durandurdu, Orthorhombic intermediate phases for the wurtzite-to-rocksalt phase transformation of CdSe: An ab initio constant pressure study. Chem. Phys. **369**(2–3), 55–58 (2010)
29. C. Kürkçü, Z. Merdan, H. Öztürk, Theoretical calculations of high-pressure phases of NiF_2: An ab initio constant-pressure study. Russ. J. Phys. Chem. A **90**(13), 2550–2555 (2016)
30. C. Kürkçü, Z. Merdan, H. Öztürk, Pressure-induced phase transitions and structural properties of CoF_2: An ab-initio molecular dynamics study. Solid State Commun. **231**, 17–25 (2016)
31. F. Birch, Finite elastic strain of cubic crystals. Phys. Rev. **71**(11), 809 (1947)
32. F. Murnaghan, The compressibility of media under extreme pressures. Proc. Natl. Acad. Sci. USA **30**(9), 244 (1944)
33. I.O.A. Ali, D.P. Joubert, M.S.H. Suleiman, A theoretical investigation of structural, mechanical, electronic and thermoelectric properties of orthorhombic $CH_3NH_3PbI_3$. Eur. Phys. J. B **91**(10), 263 (2018)
34. R. Rahmani et al., Systematic study of elastic, electronic, and magnetic properties of lanthanum cobaltite oxide. J. Comput. Electron. **17**(3), 920–925 (2018)
35. S. Li, H. Quan, S. Yu, Structural, electronic, and elastic properties of orthorhombic NaB_3H_8: a first-principles investigation. Solid State Commun. **299**, 113653 (2019)
36. P.F. Weck, E. Kim, E.C. Buck, On the mechanical stability of uranyl peroxide hydrates: implications for nuclear fuel degradation. RSC Adv. **5**(96), 79090–79097 (2015)
37. M. Nan-Xi et al., Mechanical and thermodynamic properties of the monoclinic and orthorhombic phases of SiC_2N_4 under high pressure from first principles. Chin. Phys. B **23**(12), 127101 (2014)

38. S. Al et al., Lattice dynamic properties of Rh_2 XAl (X= Fe and Y) alloys. Physica B **531**, 16–20 (2018)
39. P. Li et al., First-principles investigations on structural stability, elastic and electronic properties of Co_7M_6 (M= W, Mo, Nb) μ phases. Mol. Simul. **45**(9), 752–758 (2019)
40. Pugh, S.F., *XCII. Relations between the elastic moduli and the plastic properties of polycrystalline pure metals.* Philosophical Magazine and Journal of Science, 1954. **45**(367): p. 823–843.
41. Bannikov, V.V., I.R. Shein, and A.L. Ivanovskii, *Electronic structure, chemical bonding and elastic properties of the first thorium-containing nitride perovskite* $TaThN_3$. Physica status solidi (RRL) – Rapid Research Letters, 2007. **1**(3): p. 89–91.